AGU PUBLICATIONS

JGR

Journal of Geophysical Research: Space Physics

RESEARCH ARTICLE

10.1002/2013JA019717

Key Points:

- Helium cyclotron waves can be driven downstream of shocks
- He^{2+} can be scattered to be a shell-like distribution downstream
- Proton cyclotron waves can be excited downstream

Correspondence to:
Q. Lu,
qmlu@ustc.edu.cn

Citation:
Hao, Y., Q. Lu, X. Gao, C. Huang, S. Lu, L. Shan, and S. Wang (2014), He^{2+} dynamics and ion cyclotron waves in the downstream of quasi-perpendicular shocks: 2-D hybrid simulations, *J. Geophys. Res. Space Physics*, *119*, 3225–3236, doi:10.1002/2013JA019717.

Received 19 DEC 2013
Accepted 9 APR 2014
Accepted article online 12 APR 2014
Published online 2 MAY 2014

He^{2+} dynamics and ion cyclotron waves in the downstream of quasi-perpendicular shocks: 2-D hybrid simulations

Yufei Hao[1], Quanming Lu[1], Xinliang Gao[1], Can Huang[1], San Lu[1], Lican Shan[1], and Shui Wang[1]

[1]CAS Key Laboratory of Geospace Environment, Department of Geophysics and Planetary Science, University of Science and Technology of China, Hefei, China

Abstract The free energy provided by the ion temperature anisotropy is considered to be the source of ion cyclotron waves in the downstream of a quasi-perpendicular shock. Besides the proton cyclotron waves excited by the proton temperature anisotropy, He^{2+} is decelerated differentially from the protons by the shock due to its different charge-to-mass ratio and forms a bunched ring-like distribution in the immediate downstream of the quasi-perpendicular shock. However, how the helium cyclotron waves associated with the anisotropic distribution of He^{2+} are excited is still in debate. In this paper, with two-dimensional (2-D) hybrid simulations, we investigate He^{2+} dynamics and its role in the ion cyclotron waves downstream of quasi-perpendicular shocks (the proton plasma beta in the upstream is 0.4). A bunched ring-like distribution of He^{2+} is formed in the immediate downstream of the quasi-perpendicular shocks; then it evolves into a shell-like distribution. At last, a bi-Maxwellian distribution of He^{2+} is generated in the far downstream. In the medium and low Mach number shocks, besides the proton cyclotron waves excited near the shock front, there is another enhancement of the magnetic fluctuations in the downstream. The results show that the helium cyclotron waves can be driven directly by the bunched ring-like distribution of He^{2+} in a low or medium Mach number quasi-perpendicular shock. The relevance of our simulation results to the satellite observations is also discussed in this paper.

1. Introduction

Collisionless shocks are ubiquitous phenomena in the heliosphere from the outer solar corona [*Rosner et al.*, 1978; *Kohl et al.*, 1998] to the termination shock [*Decker et al.*, 2005; *Stone et al.*, 2005], where the upstream bulk flow energy is dissipated into the energy of the heated plasma and enhanced magnetic field [*Leroy et al.*, 1981, 1982; *Quest et al.*, 1983; *Forslund et al.*, 1984; *Lembège and Savoini*, 1992; *Anderson and Fuselier*, 1993; *Yang et al.*, 2009b]. According to the shock angle θ_{Bn} (the shock angle θ_{Bn} is defined as the angle between the shock normal and the upstream magnetic field), the shocks can be separated into two categories: quasi-parallel shocks ($\theta_{Bn} \leq 45°$) and quasi-perpendicular shocks ($\theta_{Bn} \geq 45°$) [*Jones and Ellison*, 1991]. The quasi-parallel and quasi-perpendicular shocks have quite different characteristics [*Leroy et al.*, 1982; *Livesey et al.*, 1982; *Sckopke et al.*, 1983; *Burgess*, 1989; *Lembège and Savoini*, 1992; *Schwartz et al.*, 1992; *Lembège et al.*, 1999; *Bale et al.*, 2005; *Burgess et al.*, 2005; *Lembège et al.*, 2009]. In a quasi-parallel shock, the reflected upstream ions by the shock can move far upstream along the magnetic field, then low-frequency plasma waves are excited by the plasma beam instability [*Kan and Swift*, 1983; *Scholer and Burgess*, 1992; *Schwartz et al.*, 1992; *Burgess et al.*, 2005; *Su et al.*, 2012a, 2012b]. In a quasi-perpendicular shock, the reflected upstream ions move back to the shock immediately due to their gyromotions in the upstream magnetic field and then transmit into the downstream [*Leroy et al.*, 1982; *Lembège and Savoini*, 1992; *Lembège et al.*, 2004; *Bale et al.*, 2005; *Yang et al.*, 2009a, 2012]. During this process, the reflected ions are energized in the perpendicular direction, and then they have an anisotropic distribution with the perpendicular temperature larger than the parallel one near the shock front [*Lembège and Savoini*, 1992; *Hada et al.*, 2003; *Lembège et al.*, 2004; *Yang et al.*, 2009b, 2012].

Both the linear theory [*Gary et al.*, 1976; *Gary*, 1992; *Gary et al.*, 1994] and simulations [*McKean et al.*, 1992a, 1992b, 1994] have shown that such an anisotropic distribution is unstable to ion cyclotron waves and mirror waves. According to the linear theory, the transverse ion cyclotron waves have the maximum growth rate along the background magnetic field, while the compressive mirror waves have the maximum growth rate at the wave vector oblique to the background magnetic field. In general, the ion cyclotron waves are easier to be excited in a low-beta plasma system ($\beta_{\|p} \leq 6$, where $\beta_{\|p}$ is the proton parallel plasma beta) with a large temperature anisotropy ($T_{\perp p}/T_{\|p} \geq 2$, where $T_{\perp p}$ and $T_{\|p}$ are the proton temperatures perpendicular and parallel to the background magnetic field, respectively). On the contrary, in a high-beta plasma system with a low-temperature anisotropy the mirror waves will dominate over the ion cyclotron waves [*Gary et al*., 1976; *Gary*, 1992]. Observational evidence of both the ion cyclotron waves and mirror waves has been identified in the magnetosheath behind a quasi-perpendicular shock [*Anderson et al*., 1991; *Fuselier et al*., 1991; *Lacombe et al*., 1992; *Anderson and Fuselier*, 1993].

With two-dimensional (2-D) hybrid simulations of a supercritical quasi-perpendicular shock, [*Winske and Quest*, 1988] found that during the relaxation of the anisotropic ion distribution formed due to the reflected ions by the shock, only the ion cyclotron waves are excited, which leads to the isotropization of the ion distribution. Also with 2-D hybrid simulations, *McKean et al*. [1995a] identified both the ion cyclotron waves and mirror waves in the magnetosheath behind a supercritical quasi-perpendicular shock. These waves are generated near the shock front and then convected to the downstream. In these hybrid simulations, only the protons are considered. However, besides the protons, there also exist many kinds of minor ions in the solar wind. Among these minor ions, He^{2+} is the most important ion species, which typically constitutes about 4% of the total ion density in number. With 2-D hybrid simulations, *McKean et al*. [1995b, 1996] studied the wave evolution in the downstream of low and high Mach number quasi-perpendicular shocks, where the dynamics of He^{2+} is also considered. In a high Mach number shock [*McKean et al*., 1995b], both the proton cyclotron waves and mirror waves are excited near the shock front, and then they are convected to the downstream. During such a process He^{2+} can be heated through the absorption of the proton cyclotron waves, although their contributions to the wave activities are negligible. In a low Mach number shock [*McKean et al*., 1996], only the proton cyclotron waves are excited near the shock front, which are then convected to the downstream. The helium cyclotron waves can be excited after He^{2+} is heated in the perpendicular direction through the absorption of the energy from the proton cyclotron waves and becomes gyrotropic.

The protons and He^{2+} are decelerated differently due to their different charge-to-mass ratios when they cross the electrostatic potential at a quasi-perpendicular shock. Then, a ring-beam distribution of He^{2+} may be formed in the downstream of the shock [*Fuselier and Schmidt*, 1997; *Lu and Wang*, 2006]. With one-dimensional hybrid simulations in a homogeneous plasma, *Lu and Wang* [2005] found that such a ring-beam distribution of He^{2+} can drive the helium cyclotron waves, which then scatter He^{2+} into a shell-like distribution. Both the ring-beam and shell-like distributions of He^{2+} have been observed in the downstream of a quasi-perpendicular shock [*Fuselier et al*., 1988; *Fuselier and Schmidt*, 1994, 1997], which indicates the excitation of the helium cyclotron waves by the ring-beam distribution of He^{2+} [*Lu and Wang*, 2006]. However, in the works of *Lu and Wang* [2005, 2006], the shock is not included. In this paper, with 2-D hybrid simulations, we investigate the evolutions of the waves and He^{2+} distribution in quasi-perpendicular shocks, where the shocks are generated self-consistently. It is demonstrated that in the immediate downstream of the shocks, He^{2+} has a bunched ring-like distribution after they cross the shock. The distribution can excite the helium cyclotron waves in the medium and low Mach number shocks, which scatter He^{2+} into a shell-like distribution and at last a nearly bi-Maxwellian distribution is formed in the far downstream.

This paper is organized as follow: In section 2, the 2-D hybrid simulation model is described. We present the simulation results in the section 3. And a summary and discussion is given in the last section.

2. Simulation Model

Two-Dimensional hybrid simulations are performed in the $x-y$ plane to investigate the evolution of the waves and associated He^{2+} distribution in quasi-perpendicular shocks under different Mach numbers. In the hybrid simulation model, the ions are treated kinetically and electrons as massless fluid [*Winske and Leroy*, 1985]. The upstream magnetic field lies in the $x-y$ plane, and the shock angle is $\theta_{Bn} = 87^0$. The velocity distributions of the protons and He^{2+} satisfy the Maxwellian function with the same thermal velocity, and they are injected from the left boundary with a bulk velocity (V_{inj}) along the x direction. The shock is formed by reflecting the plasma at the rigid right boundary, and the periodic boundary condition is used in the y direction.

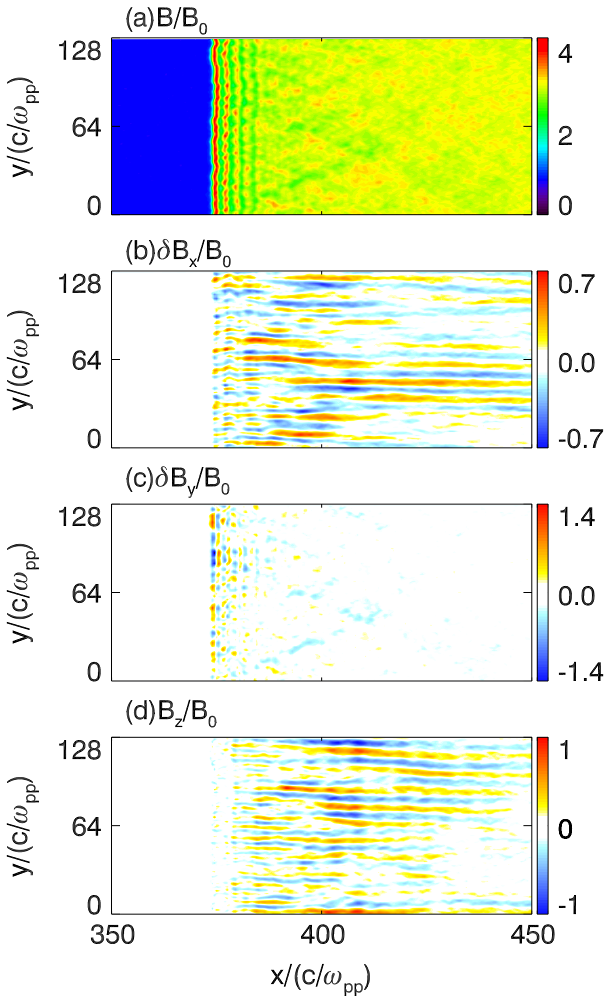

Figure 1. The contour plots of (a) the total magnetic field B/B_0, and the fluctuating magnetic field (b) $\delta B_x/B_0$, (c) $\delta B_y/B_0$, (d) B_z/B_0 at $\Omega_p t = 100$ under the medium Mach number shock condition. Here the fluctuating magnetic field is calculated as $\delta B_x = B_x - \overline{B}_x(x)$ and $\delta B_y = B_y - \overline{B}_y(x)$ ($\overline{B}_x(x)$ and $\overline{B}_y(x)$ are the corresponding average values along the y direction).

In the simulations, the units of the space and time are set as c/ω_{pp} (where the c/ω_{pp} is the proton inertial length based on the upstream parameters) and Ω_p^{-1} (where the Ω_p is the proton gyro frequency in the upstream). The proton plasma beta in the upstream is $\beta_p = 2\mu_0 p_0/B_0^2 = 0.4$(where p_0 is the upstream pressure, and B_0 is the magnetic field in the upstream). The electron beta in the upstream is set to be equal to that of the proton $\beta_e = \beta_p = 0.4$. The electron resistive length, which is define as $L_\eta = \eta c^2/(4\pi V_A)$ (where η represents wave-particles effects due to high frequency plasma instabilities), is chosen as $L_\eta = 0.1c/\omega_{pp}$. The number density of He^{2+} is chosen to be $n_\alpha = 0.04 n_e$ (where n_e is the electron density). The number of the grid cell is $n_x \times n_y = 1024 \times 128$, and the grid sizes are $\Delta x = 0.5c/\omega_{pp}$ and $\Delta y = 1.0c/\omega_{pp}$. There are 48 particles per cell on average for each ion species in the simulation domain. The time step is $\Omega_p \Delta t = 0.02$.

3. Simulation Results

A series of 2-D hybrid simulations are performed in this paper to study the effects of He^{2+} dynamics on the magnetic fluctuations under quasi-perpendicular shock conditions. The plasma are injected from the left boundary with three different speeds, which are 2.0, 3.0, and $5.0V_A$ in the simulation frame (the downstream frame), respectively. Considering that the shocks are formed by reflecting the plasma at the rigid right boundary and they propagate to the left, the Mach numbers in the shock frame are 3.2, 4.1, and 6.9, respectively.

Figure 1 shows the contour plots of (a) the total magnetic field B/B_0, and the fluctuating magnetic field (b) $\delta B_x/B_0$, (c) $\delta B_y/B_0$, (d) B_z/B_0 at $\Omega_p t = 100$ under the medium Mach number shock condition with He^{2+}. Here the fluctuating magnetic field is calculated as $\delta B_x = B_x - \overline{B}_x(x)$ and $\delta B_y = B_y - \overline{B}_y(x)$ ($\overline{B}_x(x)$ and $\overline{B}_y(x)$ are the corresponding average values along the y direction). The shock front is around $x = 375c/\omega_{pi}$, where the total magnetic field B is raised from $\sim B_0$ to $\sim 3.0B_0$. Magnetic fluctuations can be obviously observed in the downstream of the shock. The magnetic fluctuations of δB_y in the immediate downstream are resulted from spatially periodic variations of the pressure of the transmitted ions [*Ofman et al*., 2009; *Ofman and Gedalin*, 2013]. Magnetic fluctuations of δB_x and B_z are the results of the ion cyclotron waves excited by the temperature anisotropy ($T_\perp/T_\parallel > 1$, where $T_\perp$ and $T_\parallel$ are the temperatures perpendicular and parallel to the background magnetic field) [*Winske and Quest*, 1988; *McKean et al*., 1995a], which belong to the transverse modes. They are propagating along the background magnetic field. The excitation of the ion cyclotron waves in the downstream of a quasi-perpendicular shock has also been reported in previous works [*McKean et al*.,

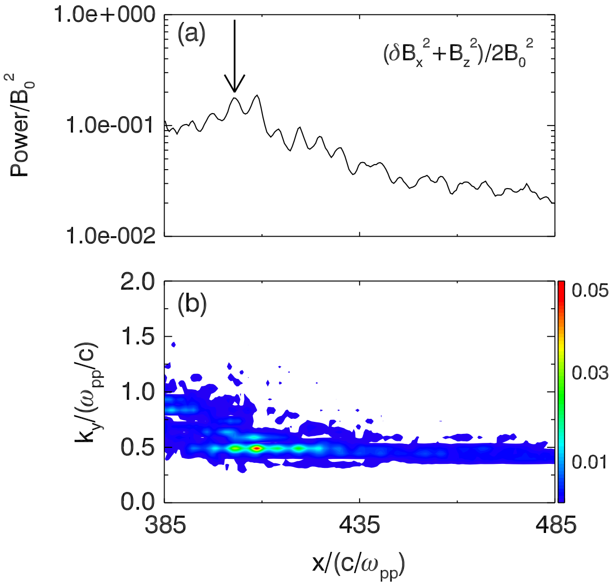

Figure 2. (a) The profile of $0.5\left(\delta B_x^2+B_z^2\right)/B_0^2$ and (b) the power spectrum of the fluctuating magnetic field $\left|B_z\left(k_y\right)\right|^2/B_0^2$ in the downstream at $\Omega_p t=100$ under the medium Mach number shock condition with He^{2+}. Here the fluctuating magnetic field $\delta B_x^2+B_z^2$ is the corresponding average value along the y direction, and $|B_z(k_y)|^2$ is obtained by Fourier transforming the different values of B_z along the y direction at a selected position x. The arrow denotes the enhancement of the magnetic fluctuations corresponding to the helium cyclotron waves. The shock front is around $x=375c/\omega_{pi}$.

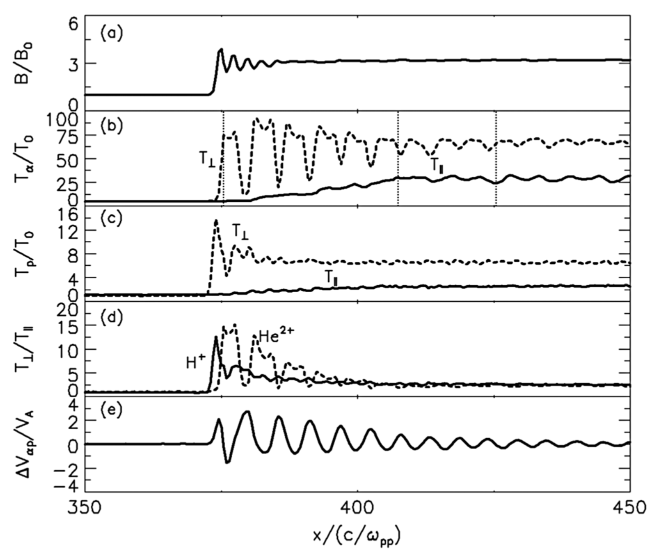

Figure 3. (a) The total magnetic field B/B_0, (b) the parallel and perpendicular temperatures of He^+ ($T_{\perp\alpha}/T_0$ and $T_{||\alpha}/T_0$, where T_0 is the upstream temperature of the protons), (c) the parallel and perpendicular temperatures of H^+ ($T_{\perp p}/T_0$ and $T_{||p}/T_0$), (d) the temperature anisotropies of He^{2+} and the protons ($T_{\perp\alpha}/T_{||\alpha}$ and $T_{\perp p}/T_{||p}$), and (e) the relative drift velocity between He^{2+} and the protons in the x direction ($\Delta V_{\alpha p}/V_A$) at $\Omega_p t=100$ under the medium Mach number shock condition with He^{2+}.

1995a, 1995b, 1996]. In general, the temperature anisotropy can excite the ion cyclotron waves and mirror waves [*Gary et al.*, 1976; *Gary*, 1992; *McKean et al.*, 1992b]. The mirror waves are compressive modes, however, in our simulations we cannot find the anti-correlation between the fluctuating magnetic field δB_y and the plasma density n. Therefore, we can eliminate the existence of the mirror waves in this run. It is consistent with the theoretical prediction, where the mirror waves can only be excited by the temperature anisotropy in plasma with a high beta, while in our simulation the plasma beta in the downstream $\beta_{||p}\sim 0.1-0.3$.

Figure 2 plots (a) the profile of 0.5 $\left(\delta B_x^2+B_z^2\right)/B_0^2$ and (b) the power spectrum of the fluctuating magnetic field $\left|B_z\left(k_y\right)\right|^2/B_0^2$ at $\Omega_p t=100$ under the medium Mach number shock condition with He^{2+}. Here the fluctuating magnetic field $\delta B_x^2+B_z^2$ is the corresponding average value along the y direction, and $|B_z(k_y)|^2$ is obtained by Fourier transforming the different values of B_z along the y direction at a selected position x. The fluctuating magnetic field is enhanced greatly around the shock front, and the dominant wave number (the amplitude of the fluctuating magnetic field has the maximum value at this wave number) is around $k_y c/\omega_{pp}\sim 0.85$. However, around $x=400c/\omega_{pp}$ we can find another enhancement of the fluctuating magnetic field with the domain wave number around $k_y c/\omega_{pp}\sim 0.50$.

In order to analyze the generation mechanism of the fluctuating magnetic field excited by the ion cyclotron waves in the downstream of the shock, in Figure 3, we display (a) the total magnetic field B/B_0, (b) the parallel and perpendicular temperatures of He^+ ($T_{\perp\alpha}/T_0$ and $T_{||\alpha}/T_0$, where T_0 is the proton temperature in the upstream), (c) the parallel and perpendicular temperatures of the protons ($T_{\perp p}/T_0$ and $T_{||p}/T_0$), (d) the temperature anisotropies of He^{2+} and the protons ($T_{\perp\alpha}/T_{||\alpha}$ and $T_{\perp p}/T_{||p}$), and

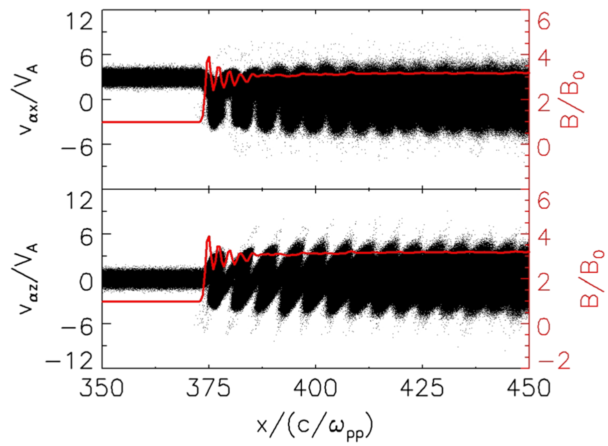

Figure 4. The $x - v_{\alpha x}$ and $x - v_{\alpha z}$ phase diagrams of He^{2+} at $\Omega_p t = 100$ under the medium Mach number shock condition with He^{2+}. The total magnetic field are presented (denoted with red lines) for reference.

(e) the relative drift velocity between He^{2+} and the protons in the x direction ($\Delta V_{\alpha p}/V_A$) at $\Omega_p t = 100$ under the medium Mach number shock with He^{2+}. Here the parallel and perpendicular temperatures are calculated with the following method: the parallel temperature $T_{||} = m_i\langle(v_y - \langle v_y\rangle)^2\rangle$ and the perpendicular temperature $T_\perp = m_i\langle(v_x - \langle v_x\rangle)^2 + (v_z - \langle v_z\rangle)^2\rangle/2$ are at first calculated in every grid cell (where the bracket $\langle\bullet\rangle$ denotes an average over one grid cell), and the temperatures shown in the figure are the average values along the y direction. A part of the upstream protons are reflected by the shock and then are energized in the perpendicular direction. These particles eventually transmit into the downstream; therefore, the distribution of the protons in the downstream is anisotropic, which has been investigated in previous works [*Leroy et al.*, 1982; *Lembège and Savoini*, 1992; *Hada et al.*, 2003]. The proton cyclotron waves are excited during the relaxation of the anisotropic distribution.

For He^{2+}, they are decelerated differentially from the protons by the shock due to their different charge-to-mass ratios. These particles will gyrate in the background magnetic field and form a bunched ring-like distribution. This can be demonstrated in Figure 4, which plots the $x - v_{\alpha x}$ and $x - v_{\alpha z}$ phase diagrams of He^{2+} at $\Omega_p t = 100$ under the medium Mach number shock condition with He^{2+}. Such a distribution leads to a large variation of the He^{2+} temperature in the downstream of the shock, which is shown in Figure 3. The evolution of the He^{2+} distributions at different positions at $\Omega_p t = 100$ under the medium Mach number shock condition is depicted in Figure 5. The bunched ring-like distribution is formed in the immediate downstream (Figure 5a), and it is unstable to the helium cyclotron waves, which is similar to that of a ring-beam distribution [*Lu and Wang*, 2005, 2006]. Because He^{2+} has a smaller charge-to-mass ratio than the proton, the helium will take more time to grow to a large amplitude. Therefore, the enhancement of the fluctuating magnetic field with the dominant wave number around $k_y c/\omega_{pp} \sim 0.50$ (excited due to the

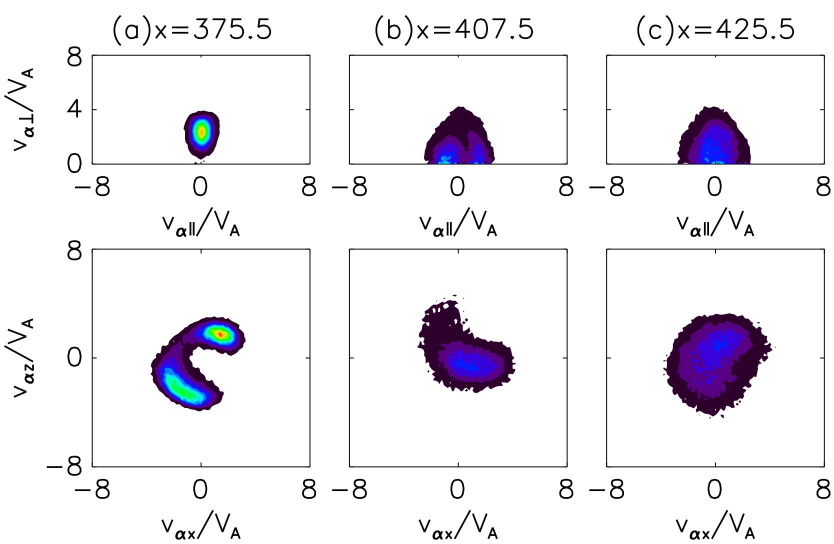

Figure 5. The velocity distributions of He^{2+} in the (top) $v_{\alpha||} - v_{\alpha\perp}$ and (bottom) $v_{\alpha x} - v_{\alpha z}$ planes at $\Omega_p t = 100$ under the medium Mach number shock condition with He^{2+}. (a) $x = 375.5c/\omega_{pp}$, (b) $x = 407.5c/\omega_{pp}$, and (c) $x = 425.5c/\omega_{pp}$ with two grid cells in the x direction and all the grid cells in they direction.

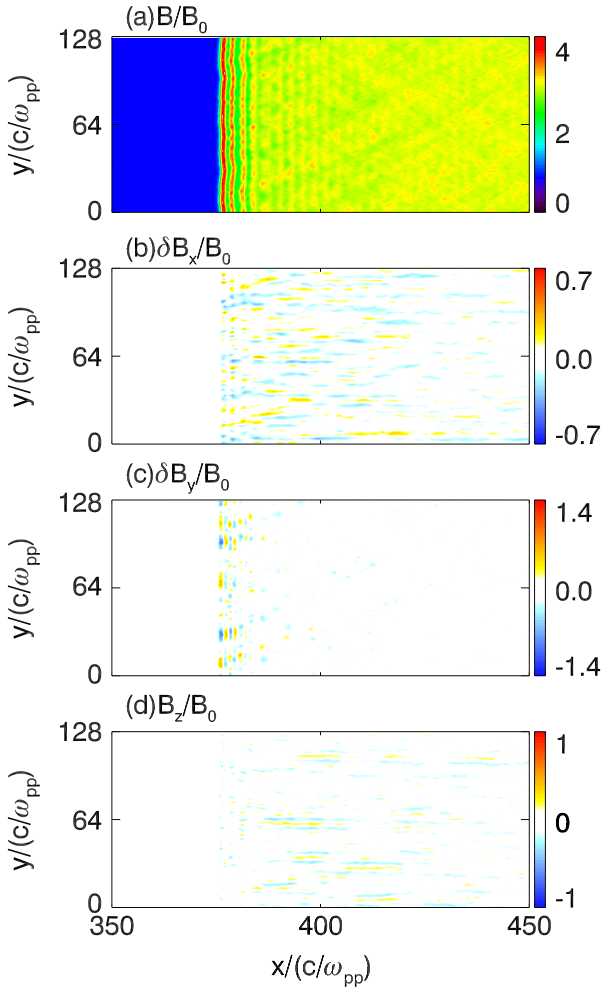

Figure 6. The contours of (a) the total magnetic field B/B_0, and the fluctuating magnetic field (b) $\delta B_x/B_0$, (c) $\delta B_y/B_0$, (d) B_z/B_0 at $\Omega_p t=100$ under the medium Mach number shock condition without He^{2+} ions. Here the fluctuating magnetic field is calculated as $\delta B_x = B_x - \overline{B}_x(x)$ and $\delta B_y = B_y - \overline{B}_y(x)$ ($\overline{B}_x(x)$ and $\overline{B}_y(x)$ are the corresponding average values along the y direction).

helium cyclotron waves) are in the further downstream than that with the dominant wave number around $k_y c/\omega_{pp} \sim 0.85$ (excited due to the proton cyclotron waves), as shown in Figure 2. With the excitation of the helium cyclotron waves, the bunched ring-like distribution is scattered to a shell-like distribution (Figure 5b), and finally, it evolves into a bi-Maxwellian distribution in the far downstream. The formation of the shell-like distribution is due to the scattering of the particles by the helium cyclotron waves with both negative and positive wave numbers, which is similar to the situation described in *Tanaka* [1985].

To distinguish the role of He^{2+} in the downstream waves of a quasi-perpendicular shock. We also perform runs without He^{2+} ions and keep other parameters as the same. Figure 6 shows the contours of (a) the total magnetic field B/B_0, and the fluctuating magnetic field (b) $\delta B_x/B_0$, (c) $\delta B_y/B_0$, (d) B_z/B_0 at $\Omega_p t=100$ under the medium Mach number shock condition without He^{2+}. As in Figure 1, the fluctuating magnetic field is calculated as $\delta B_x = B_x - \overline{B}_x(x)$ and $\delta B_y = B_y - \overline{B}_y(x)$ ($\overline{B}_x(x)$ and $\overline{B}_y(x)$ are the corresponding average values along the y direction). The shock front is also around $x=375c/\omega_{pi}$, and the total magnetic field B is raised from $\sim B_0$ to $\sim 3.0B_0$. The existence of He^{2+} has obvious impact on the evolution of downstream waves. Compared with the run with He^{2+}, here the amplitude of the downstream waves is obviously smaller. Figure 7 plots (a) the profile of $0.5\left(\delta B_x^2 + B_z^2\right)/B_0^2$ and (b) the power spectrum of the fluctuating magnetic field $\left|B_z\left(k_y\right)\right|^2/B_0^2$ at $\Omega_p t=100$ under the medium Mach number shock condition without He^{2+}. The fluctuating magnetic field is enhanced only in the immediate downstream, which is excited due to the proton temperature anisotropy formed by the reflected protons at the shock front.

In summary, under the medium Mach number quasi-perpendicular shock condition, He^{2+} plays an important role in the downstream waves. After crossing the shock, He^{2+} first forms a bunched ring-like distribution, which is unstable to the helium cyclotron waves. Therefore, we can observe another enhancement of the fluctuating magnetic field in the downstream. At the same time, the helium cyclotron waves can scatter He^{2+} to a shell-like distribution, and at last a bi-Maxwellian distribution is generated. A shell-like distribution of He^{2+} was previously observed in the downstream of a quasi-perpendicular shock [*Fuselier et al.*, 1988].

To further investigate the role of He^{2+} in a quasi-perpendicular shock, we have also performed the runs under the low and high Mach number shock. Figure 8 shows the fluctuating magnetic field B_z/B_0, the power spectrum of the fluctuating magnetic field $\left|\delta B_z\left(k_y\right)\right|^2/B_0^2$ and the profile of $0.5\left(\delta B_x^2 + B_z^2\right)/B_0^2$ at $\Omega_p t=100$ under the low Mach number shock condition, (a) with He^{2+} and (b) without He^{2+}. The shock is around

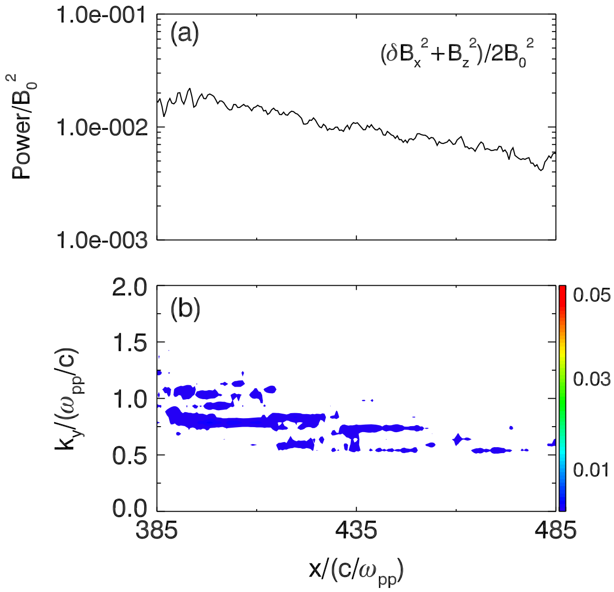

Figure 7. (a) The profile of $0.5\left(\delta B_x^2+B_z^2\right)/B_0^2$ and (b) the power spectrum of the fluctuating magnetic field $\left|B_z\left(k_y\right)\right|^2/B_0^2$ in the downstream at $\Omega_p t = 100$ under the medium Mach number shock condition without He^{2+}. Here the fluctuating magnetic field $\delta B_x^2+B_z^2$ is the corresponding average value along the y direction, and $|B_z(k_y)|^2$ is obtained by Fourier transforming the different values of B_z along the y direction at a selected position x. The arrow denotes the enhancement of the magnetic fluctuations corresponding to the helium cyclotron waves.

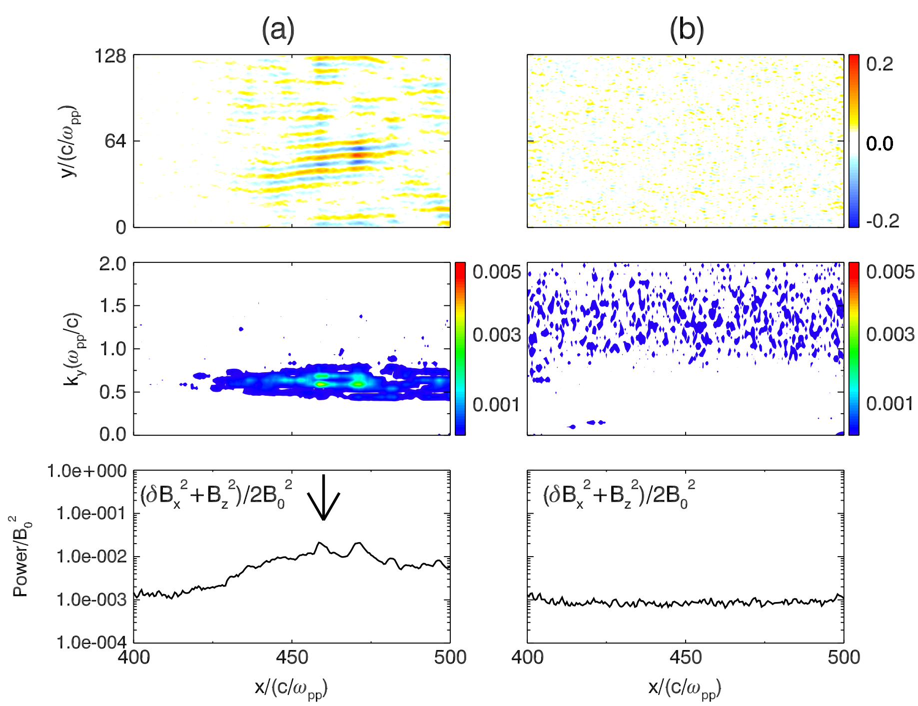

Figure 8. The contours of (top) the fluctuating magnetic field B_z/B_0, (middle) the power spectrum of the fluctuating magnetic field $\left|\delta B_z\left(k_y\right)\right|^2/B_0^2$, and (bottom) the profile of $0.5\left(\delta B_x^2+B_z^2\right)/B_0^2$ in the downstream at $\Omega_p t = 100$ under the low Mach number shock condition, (a) with He^{2+} ions and (b) without He^{2+} ions. In Figure 8 (middle), the fluctuating magnetic field $\delta B_x^2+B_z^2$ is the corresponding average value along the y direction, and in Figure 8 (bottom) $|B_z(k_y)|^2$ is obtained by Fourier transforming the different values of B_z along the y direction at a selected position x. The arrow denotes the enhancement of the magnetic fluctuations corresponding to the helium cyclotron waves. The shock is around $x = 392c/\omega_{pp}$.

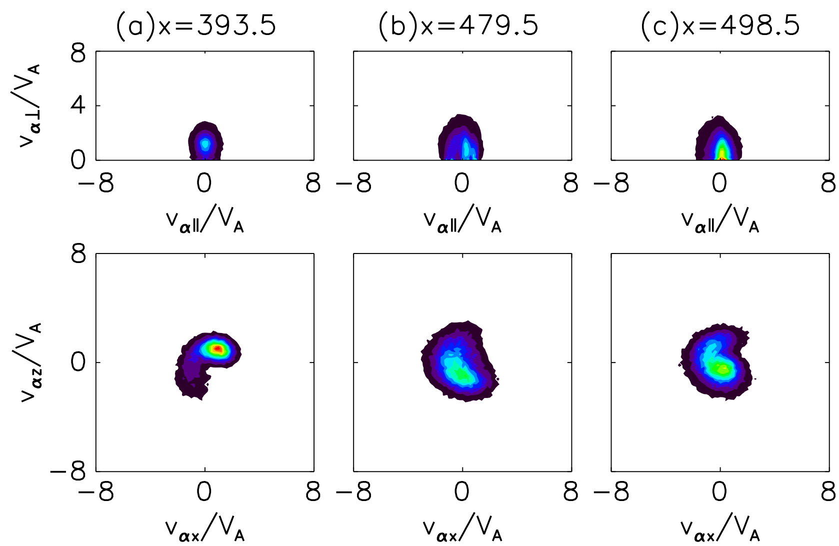

Figure 9. The velocity distributions of He^{2+} in the (top) $v_{\alpha||} - v_{\alpha\perp}$ and (bottom) $v_{\alpha x} - v_{\alpha z}$ planes at $\Omega_p t = 100$ under the low Mach number shock condition with He^{2+}. (a) $x = 393.5c/\omega_{pp}$, (b) $x = 479.5c/\omega_{pp}$, and (c) $x = 498.5c/\omega_{pp}$ with two grid cells in the x direction and all the grid cells in the y direction.

$x = 392c/\omega_{pp}$, which is not shown in the figure. In the run without He^{2+}, we cannot observe strong waves in the downstream. However, in the run with He^{2+}, obvious enhancement of the magnetic fluctuations can be observed from about $x = 460c/\omega_{pp}$ with the dominant wave number around $k_y c/\omega_{pp} \sim 0.63$. Figure 9 plots the evolution of the He^{2+} distributions at different positions at $\Omega_p t = 100$ under the low Mach number shock condition with He^{2+}. In the immediate downstream of the shock, the He^{2+} distribution satisfies the bunched ring-like function

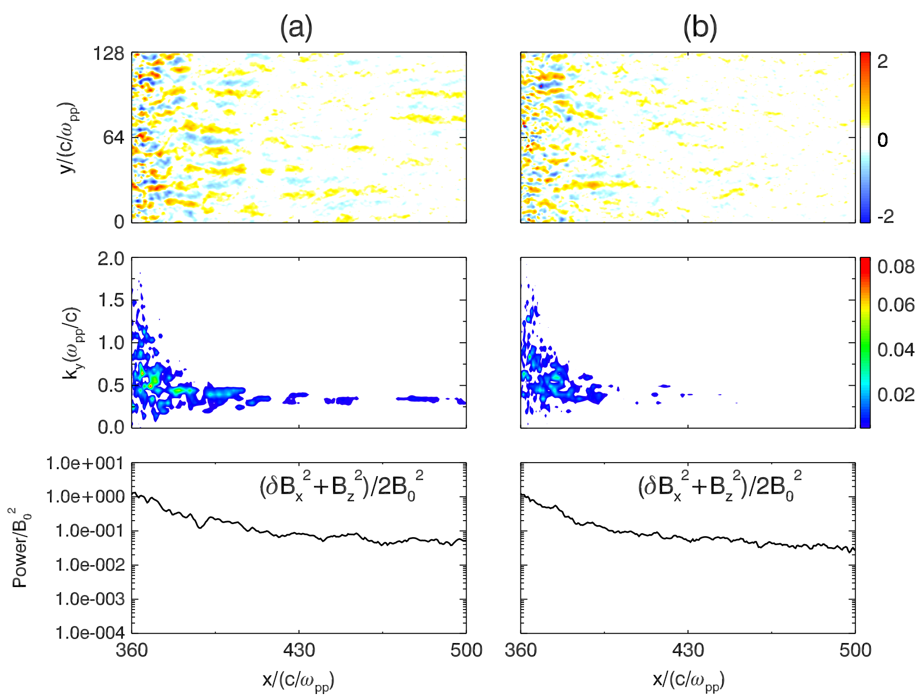

Figure 10. The contours of (top) the fluctuating magnetic field B_z/B_0, (middle) the power spectrum of the fluctuating magnetic field $\left|\delta B_z(k_y)\right|^2/B_0^2$, and (bottom) the profile of $0.5\left(\delta B_x^2 + B_z^2\right)/B_0^2$ in the downstream at $\Omega_p t = 80$ under the high Mach number shock condition, (a) with He^{2+} ions and (b) without He^{2+} ions. In Figure 10 (middle), the fluctuating magnetic field $\delta B_x^2 + B_z^2$ is the corresponding average value along the y direction, and in Figure 10 (bottom) $|B_z(k_y)|^2$ is obtained by Fourier transforming the different values of B_z along the y direction at a selected position x. The shock is around $x = 357c/\omega_{pp}$.

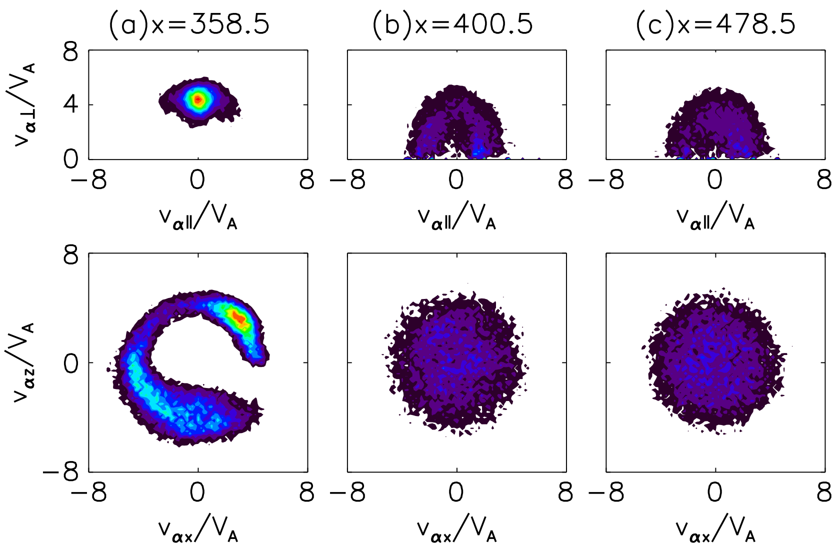

Figure 11. The velocity distributions of He^{2+} in the (top) $v_{\alpha||} - v_{\alpha\perp}$ and (bottom) $v_{\alpha x} - v_{\alpha z}$ planes at $\Omega_p t = 80$ under the high Mach number shock condition with He^{2+}. (a) $x = 358.5c/\omega_{pp}$, (b) $x = 400.5c/\omega_{pp}$, and (c) $x = 478.5c/\omega_{pp}$ with two grid cells in the x direction and all the grid cells in the y direction.

(Figure 9a). Similar to the run under the medium Mach number shock condition, with the enhancement of the magnetic fluctuations, the He^{2+} distribution is first scattered to a shell-like (Figure 9b), and then a bi-Maxwellian function in the far downstream (Figure 9c). Therefore, the magnetic fluctuations observed in the run with He^{2+} correspond to the helium cyclotron waves excited by the bunched ring-like distribution of He^{2+}.

Figure 10 shows the fluctuating magnetic field B_z/B_0, the power spectrum of the fluctuating magnetic field $\left|\delta B_z\left(k_y\right)\right|^2/B_0^2$ and the profile of $0.5\left(\delta B_x^2 + B_z^2\right)/B_0^2$ at $\Omega_p t = 80$ under the high Mach number shock condition, (a) with He^{2+} and (b) without He^{2+}. The shock is around $x = 357c/\omega_{pp}$, which is also not shown in the figure. The existence of He^{2+} doesn't have obvious impact on the evolution of the ion cyclotron waves in the downstream. However, in Figure 11, the bunched ring-like distribution also emerges in the immediate downstream (Figure 11a). It then evolves in to a shell-like distribution (Figure 11b) until to a bi-Maxwell distribution in the far downstream (Figure 11c). However, in the high Mach number shock, the proton cyclotron waves excited due to the proton temperature anisotropy is very strong, and we cannot observe obvious enhancement of the magnetic fluctuations, which corresponds to the helium cyclotron waves. The existence of the shell-like distribution for He^{2+} in the downstream are scattered by the helium cyclotron waves or proton cyclotron waves from the bunched ring-like distribution. At the same time, under the high Mach number shock condition, the mirror waves can also be excited. This can be demonstrated in Figure 12, which shows (a) the magnetic field $\delta B_y/B_0$ and (b) the correlation coefficient of the

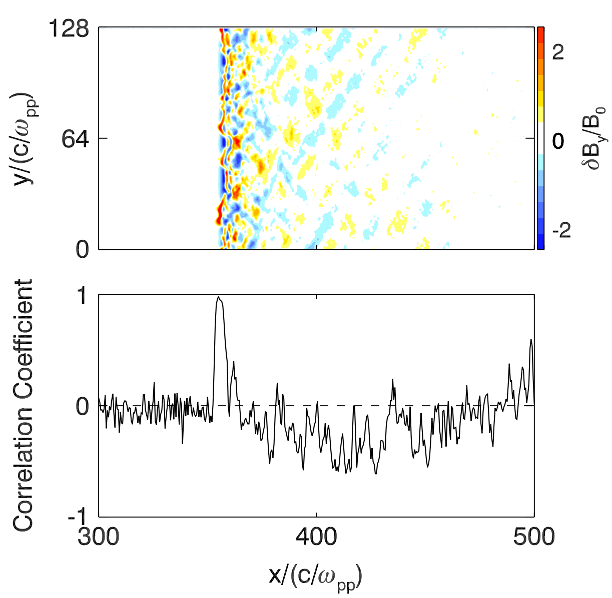

Figure 12. (a) The magnetic field $\delta B_y/B_0$, and (b) the correlation coefficient of the proton density and total magnetic field averaged over the y direction at $\Omega_p t = 80$ under the high Mach number shock condition with He^{2+} ions.

proton density and total magnetic field averaged over the y direction at $\Omega_p t = 80$ under the high Mach number shock condition with He^{2+}. The shock front is also around $x = 357c/\omega_{pp}$. The correlation coefficient is around -0.5 from about $x = 380c/\omega_{pp}$to $x = 450c/\omega_{pp}$. That is, the plasma number density is negatively correlated with the total magnetic field, which infers the existence of the mirror waves. Therefore, the fluctuations of δB_y correspond to the mirror waves excited by the proton temperature anisotropy. Also, here the existence of He^{2+} does not have obvious influence on the mirror waves (not shown).

4. Conclusions and Discussion

In this paper, 2-D hybrid simulations are performed to investigate the role of He^{2+} in the ion cyclotron waves downstream of quasi-perpendicular shocks. Due to its different charge-to-mass ratio, He^{2+} is decelerated differentially from the protons by the shocks, which results in a bunched ring-like distribution of He^{2+} in the immediate downstream of the shocks. In medium and low Mach number shocks, besides the protons cyclotron waves excited by the proton temperature anisotropy at the shocks, there is another enhancement of magnetic fluctuations behind the proton cyclotron waves, which corresponds to the helium cyclotron waves excited by the bunched ring-like distribution of He^{2+}. On the other hand, the helium cyclotron waves can also influence the He^{2+} distribution. The bunched ring-like distribution is first scattered to a shell-like distribution, and then it evolves into a bi-Maxwell distribution. In a high Mach number shock, the bunched ring-like distribution of He^{2+} can also been scattered into a shell-like and a bi-Maxwellian distribution, and we cannot observe the obvious enhancement of the magnetic fluctuations corresponding to the helium cyclotron waves. Here the proton cyclotron waves excited in the immediate downstream is very strong, and their amplitude decreases when the waves are convected to the far downstream. Even when the helium cyclotron waves are excited, the amplitude of the proton cyclotron waves is still sufficiently strong, and we cannot observe an obvious enhancement of the fluctuating magnetic field in the downstream. The shell-like distribution for He^{2+} in the downstream might be formed due to the scattering either by the helium cyclotron waves or proton cyclotron waves. In addition, the mirror waves can also been driven by the proton temperature anisotropy in the downstream of the high Mach number quasi-perpendicular shock. In a high Mach number quasi-perpendicular shock, a smaller grid size in hybrid simulations may make a shock steepen to a smaller scale. Then, both the protons and He^{2+} would have larger temperature anisotropy, and the excited waves are stronger. However, it should not change our conclusions: the helium cyclotron waves can be excited in the downstream of a quasi-perpendicular shock.

In the works of *McKean et al*. [1996], the helium cyclotron waves in the downstream of a low Mach number quasi-perpendicular shock are excited after He^{2+} absorbs the energy from the proton cyclotron waves. However, our results show that only helium cyclotron waves are excited downstream in a low Mach number quasi-perpendicular shock. The shell-like distribution of He^{2+} can been formed due to the scattering of the helium cyclotron waves excited by the ring-beam distribution of He^{2+}. Active Magnetospheric Particle Tracer Explorers/CCE spacecraft observed both the ring-like and shell-like distributions in the downstream of the terrestrial bow shock under quasi-perpendicular shock conditions [*Fuselier et al*., 1988; *Fuselier and Schmidt*, 1997]. Therefore, it provides the evidence that the helium cyclotron waves may grow in the downstream of a quasi-perpendicular shock, and they are excited directly by the ring-like distribution of He^{2+}.

Acknowledgments

This research was supported by the 973 Program (2013CBA01503, 2012CB825602), and the National Science Foundation of China, grants 41174124, 41274144, 41331067, 41121003, and 11235009, and CAS Key Research Program KZZD-EW-01.

M. Balikhin thanks the reviewers for their assistance in evaluating this paper.

References

Anderson, B. J., and S. A. Fuselier (1993), Magnetic pulsations from 0.1 to 4.0 Hz and associated plasma properties in the Earth's subsolar depletion magnetosheath and plasma depletion layer, *J. Geophys. Res.*, *98*, 1461–1479, doi:10.1029/92JA02197.

Anderson, B. J., S. A. Fuselier, and D. Murr (1991), Electromagnetic ion cyclotron waves observed in the plasma depletion layer, *Geophys. Res. Lett.*, *18*, 1955–1958, doi:10.1029/91GL02238.

Bale, S. D., et al. (2005), Quasi-perpendicular shock structure and processes, *Space Sci. Rev.*, *118*, 161–203, doi:10.1007/s11214-005-3827-0.

Burgess, D. (1989), Cyclic behavior at quasi-parallel collisionless shocks, *Geophys. Res. Lett.*, *16*, 345–348, doi:10.1029/GL016i005p00345.

Burgess, D., et al. (2005), Quasi-parallel shock structure and processes, *Space Sci. Rev.*, *118*, 205–222.

Decker, R. B., S. M. Krimigis, E. C. Roelof, M. E. Hill, T. P. Armstrong, G. Gloeckler, D. C. Hamilton, and L. J. Lanzerotti (2005), Voyager 1 in the foreshock, termination shock, and heliosheath, *Science*, *309*, 2020–2024, doi:10.1126/science.1117569.

Forslund, D. W., K. B. Quest, J. U. Brackbill, and K. Lee (1984), Collisionless dissipation in quasi-perpendicular shocks, *J. Geophys. Res.*, *89*, 2142–2150, doi:10.1029/JA089iA04p02142.

Fuselier, S. A., and W. K. H. Schmidt (1994), H + and He2+ heating at the Earth's bow shock, *J. Geophys. Res.*, *99*, 11,539–11,546, doi:10.1029/94JA00350.

Fuselier, S. A., and W. K. H. Schmidt (1997), Solar wind He2+ ring-beam distributions downstream from the Earth's bow shock, *J. Geophys. Res.*, *102*, 11,273–11,280, doi:10.1029/97JA00643.

Fuselier, S. A., E. G. Shelley, and D. M. Klumpar (1988), AMPTE/CCE observations of shell-like He2+ and O6+ distributions in the magnetosheath, *Geophys. Res. Lett.*, *15*, 1333–1336, doi:10.1029/GL015i012p01333.

Fuselier, S. A., D. M. Klumpar, E. G. Shelley, B. J. Anderson, and A. J. Coates (1991), He2+ and H + dynamics in the subsolar magnetosheath and plasma depletion layer, *J. Geophys. Res.*, *96*, 21,095–21,104, doi:10.1029/91JA02145.

Gary, S. P. (1992), The mirror and ion cyclotron anisotropy instabilities, *J. Geophys. Res.*, *97*, 8519–8529, doi:10.1029/92JA00299.

Gary, S. P., M. D. Montgomery, W. C. Feldman, and D. W. Forslund (1976), Proton temperature anisotropy instabilities in the solar wind, *J. Geophys. Res.*, *81*, 1241–1246, doi:10.1029/JA081i007p01241.

Gary, S. P., M. E. McKean, D. Winske, B. J. Anderson, R. E. Denton, and S. A. Fuselier (1994), The proton cyclotron instability and the anisotropy β inverse correlation, *J. Geophys. Res.*, *99*, 5903–5914, doi:10.1029/93JA03583.

Hada, T., M. Oonishi, B. Lembège, and P. Savoini (2003), Shock front nonstationarity of supercritical perpendicular shocks, *J. Geophys. Res.*, *108*(A16), 1233, doi:10.1029/2002JA009339.

Jones, F. C., and D. C. Ellison (1991), The plasma physics of shock acceleration, *Space Sci. Rev.*, *58*(1), 259–346.

Kan, J. R., and D. W. Swift (1983), Structure of the quasi-parallel bow shock: Results of numerical simulations, *J. Geophys. Res.*, *88*, 6919–6925, doi:10.1029/JA088iA09p06919.

Kohl, J. L., et al. (1998), UVCS/SOHO empirical determinations of anisotropic velocity distributions in the solar corona, *Astrophys. J.*, *501*, L127–L131.

Lacombe, C., F. G. E. Pantellini, D. Hubert, C. C. Harvey, A. Mangeney, G. Belmont, and C. T. Russell (1992), Mirror and Alfvenic waves observed by ISEE 1–2 during crossings of the Earth's bow shock, *Ann. Geophys.*, *10*, 772.

Lembège, B., and P. Savoini (1992), Nonstationarity of a two-dimensional quasiperpendicular supercritical collisionless shock by self-reformation, *Phys. Fluids B*, *4*, 3533–3548, doi:10.1063/1.860361.

Lembège, B., S. N. Walker, P. Savoini, M. A. Balikhin, and V. Krasoselskikh (1999), The spatial sizes of electric and magnetic field gradients in simulated shocks, *Adv. Space Res.*, *24*, 109.

Lembège, B., J. Giacalone, M. Scholer, T. Hada, M. Hoshino, V. Krasnoselskikh, H. Kucharek, P. Savoini, and T. Terasawa (2004), Selected problems in collisionless-shock physics, *Space Sci. Rev.*, *110*, 161.

Lembège, B., P. Savoini, P. Hellinger, and P. Travnicek (2009), Nonstationarity of a two-dimensional perpendicular shock: Competing mechanisms, *J. Geophys. Res.*, *114*, A03217, doi:10.1029/2008JA013618.

Leroy, M. M., C. C. Goodrich, D. Winske, C. S. Wu, and K. Papadopoulos (1981), Simulation of a perpendicular bow shock, *Geophys. Res. Lett.*, *8*, 1269–1272, doi:10.1029/GL008i012p01269.

Leroy, M. M., D. Winske, C. C. Goodrich, C. S. Wu, and K. Papadopoulos (1982), The structure of perpendicular bow shocks, *J. Geophys. Res.*, *87*, 5081–5094, doi:10.1029/JA087iA07p05081.

Livesey, W. A., C. F. Kennel, and C. T. Russell (1982), ISEE-1 and -2 observations of magnetic field strength overshoots in quasi-perpendicular bow shocks, *Geophys. Res. Lett.*, *9*, 1037–1040, doi:10.1029/GL009i009p01037.

Lu, Q. M., and S. Wang (2005), Formation of He2+ shell-like distributions downstream of the Earth's bow shock, *Geophys. Res. Lett.*, *32*, L03111, doi:10.1029/2004GL021508.

Lu, Q. M., and S. Wang (2006), Electromagnetic waves downstream of quasi-perpendicular shocks, *J. Geophys. Res.*, *111*, A05204, doi:10.1029/2005JA011319.

McKean, M. E., D. Winske, and S. P. Gary (1992a), Kinetic properties of mirror waves in magnetosheath plasmas, *Geophys. Res. Lett.*, *19*, 1331–1334, doi:10.1029/92GL01282.

McKean, M. E., D. Winske, and S. P. Gary (1992b), Mirror and ion cyclotron anisotropy instabilities in the magnetosheath, *J. Geophys. Res.*, *97*, 19,421–19,432, doi:10.1029/92JA01842.

McKean, M. E., D. Winske, and S. P. Gary (1994), Two-dimensional simulations of ion anisotropy instabilities in the magnetosheath, *J. Geophys. Res.*, *99*, 11,141–11,153, doi:10.1029/93JA03025.

McKean, M. E., N. Omidi, and D. Krauss-Varban (1995a), Wave and ion evolution downstream of quasi-perpendicular bow shocks, *J. Geophys. Res.*, *100*, 3427–3437, doi:10.1029/94JA02529.

McKean, M. E., N. Omidi, D. Krauss-Varban, and H. Karimabadi (1995b), Wave and particle evolution downstream of quasi-perpendicular shocks, *Adv. Space Res.*, *15*, 319–322.

McKean, M. E., N. Omidi, and D. Krauss-Varban (1996), Magnetosheath dynamics downstream of low Mach number shocks, *J. Geophys. Res.*, *101*, 20,013–20,022, doi:10.1029/96JA01461.

Ofman, L., and M. Gedalin (2013), Two-dimensional hybrid simulations of quasi-perpendicular collisionless shock dynamics: Gyrating downstream ion distributions, *J. Geophys. Res. Space Physics*, *118*, 1828–1836, doi:10.1029/2012JA018188.

Ofman, L., M. Balikhin, C. T. Russell, and M. Gedalin (2009), Collisionless relaxation of ion distributions downstream of laminar quasi-perpendicular shocks, *J. Geophys. Res.*, *114*, A09106, doi:10.1029/2009JA014365.

Quest, K. B., D. W. Forslund, U. Brackbill, and K. Lee (1983), Collisionless dissipation processes in quasi-parallel shocks, *Geophys. Res. Lett.*, *10*, 471–474, doi:10.1029/GL010i006p00471.

Rosner, R., W. H. Tucker, and G. Vaiana (1978), Dynamics of the quiescent solar corona, *Astrophys. J.*, *220*, 643–645.

Scholer, M., and D. Burgess (1992), The role of upstream waves in supercritical quasi-parallel shock re-formation, *J. Geophys. Res.*, *97*, 8319–8326, doi:10.1029/92JA00312.

Schwartz, S. J., D. Burgess, W. P. Wilkinson, R. L. Kessel, M. Dunlop, and H. Lühr (1992), Observations of short large-amplitude magnetic structures at a quasi-parallel shock, *J. Geophys. Res.*, *97*, 4209–4227, doi:10.1029/91JA02581.

Sckopke, N., G. Paschmann, S. J. Bame, J. T. Gosling, and C. T. Russell (1983), Evolution of ion distributions across the nearly perpendicular bow shock: Specularly and non-specularly reflected-gyrating ions, *J. Geophys. Res.*, *88*, 6121–6136, doi:10.1029/JA088iA08p06121.

Stone, E. C., A. C. Cummings, F. B. McDonald, B. C. Heikkila, N. Lal, and W. R. Webber (2005), Voyager 1 explores the termination shock region and the heliosheath beyond, *Science*, *309*, 2017–2020.

Su, Y., Q. Lu, X. Gao, C. Huang, and S. Wang (2012a), Ion dynamics at supercritical quasi-parallel shocks: Hybrid simulations, *Phys. Plasmas*, *19*, 092108.

Su, Y., Q. Lu, C. Huang, M. Wu, X. Gao, and S. Wang (2012b), Particle acceleration and generation of diffuse superthermal ions at a quasi-parallel collisionless shock: Hybrid simulations, *J. Geophys. Res.*, *117*, A08107, doi:10.1029/2012JA017736.

Tanaka, M. (1985), Simulations of heavy-ion heating by electromagnetic ion-cyclotron waves driven by proton temperature anisotropies, *J. Geophys. Res.*, *90*, 6459–6468, doi:10.1029/JA090iA07p06459.

Winske, D., and M. M. Leroy (1985), Hybrid simulation techniques applied to the Earth's bow shock, in *Computer Simulation of Space Plasmas*, edited by H. M. T. Sato, pp. 255–278, Terra Sci., Tokyo, Japan.

Winske, D., and K. B. Quest (1988), Magnetic field and density fluctuations at perpendicular supercritical collisionless shocks, *J. Geophys. Res.*, *93*, 9681–9693, doi:10.1029/JA093iA09p09681.

Yang, Z. W., Q. M. Lu, B. Lembege, and S. Wang (2009a), Shock front nonstationarity and ion acceleration in supercritical perpendicular shocks, *J. Geophys. Res.*, *114*, A03111, doi:10.1029/2008JA013785.

Yang, Z. W., Q. M. Lu, and S. Wang (2009b), The evolution of the electric field at a nonstationary perpendicular shock, *Phys. Plasmas*, *16*, 124502.

Yang, Z. W., B. Lembège, and Q. M. Lu (2012), Impact of the rippling of a perpendicular shock front on ion dynamics, *J. Geophys. Res.*, *117*, A07222, doi:10.1029/2011JA017211.